ELSEVIER

International Journal of Solids and Structures 41 (2004) 717–730

INTERNATIONAL JOURNAL OF SOLIDS and STRUCTURES

www.elsevier.com/locate/ijsolstr

A theoretical and numerical study of thin film delamination using the pull-off test

Zuo Sun [a,1], Kai-Tak Wan [b], David A. Dillard [a,*]

[a] *Department of Engineering Science and Mechanics, Virginia Polytechnic Institute and State University, Blacksburg, VA 24061-0219, USA*

[b] *Department of Mechanical and Aerospace Engineering and Engineering Mechanics, University of Missouri-Rolla, Rolla, MO 65409-0050, USA*

Received 23 June 2003

Abstract

An accurate closed-form analytical solution for the strain energy release rate for a thin rectangular film loaded by a central line force using the pull-off test is derived in the presence of a tensile residual stress. The theoretical constitutive relation and the strain energy release rate agree very well with two-dimensional nonlinear finite element analysis for the entire deformation regime ranging from bending plate to stretching membrane. Fracture modes for this pull-off test are also investigated based upon the finite element analysis, offering additional insights to the interfacial delamination.

Keywords: Pull-off test; Residual stress; Strain energy release rate; Finite element analysis; Adhesion test; Coating delamination; V-peel test

1. Introduction

In recent years, thin films and coatings have been increasingly used in many widely varying applications such as automobiles, microelectronics, optical devices, and biomedical engineering. Although a thorough understanding of mechanical properties and interfacial delamination is desired to ensure the reliability, lifespan, and structural integrity of thin-film adhesion, it was not until the introduction of a fracture mechanics approach that interfacial adhesion was studied extensively and systematically. The general concepts of interfacial fracture mechanics are related to the critical strain energy release rate (fracture energy), which is the work per unit area required to separate the interface of interest. This parameter is widely used to quantify interfacial adhesion because it is a function of both material properties, such as the interface chemistry, adjacent microstructures, elastic–plastic constitutive behavior, and viscoelasticity; and

* Corresponding author. Tel.: +1-540-231-4714; fax: +1-540-231-4574.
E-mail address: dillard@vt.edu (D.A. Dillard).
[1] Current address: GE Global Research Center, Schenectady, NY, USA. *E-mail address*: sunz@research.ge.com

0020-7683/$ - see front matter © 2003 Elsevier Ltd. All rights reserved.
doi:10.1016/j.ijsolstr.2003.09.027

mechanical parameters such as the loading mixity close to the debond tip (Dauskardt et al., 1998; Hutchingson and Suo, 1992).

Many adhesion test techniques have been developed to measure adhesion energy at the interface, among which blister and peel tests are two widely used methods to test adhesion of thin films and coatings. Blister tests were originally proposed by Dannenberg (1961) for debonding a strip of coating into a cavity, and the more common circular version was introduced by Williams (1972). The method was generalized to thinner films by considering only membrane action (Bennett et al., 1974; Gent and Lewandowski, 1987; Williams, 1997) or a combination of bending and stretching (Cotterell and Chen, 1997; Sheplak and Dugundji, 1998; Wan and Lim, 1998). Jensen and Thouless (1993) also incorporated residual stress effects into the energy release rate and mode mixity determination in the blister test. In the standard or pressurized circular blister test, either a liquid or gas is applied under pressure through a hole in the substrate, forcing the coating to debond. The strain energy release rate can be calculated from the relationship between the pressure, blister radius, and blister height. However, one disadvantage of the standard blister test is that the strain energy release rate increases as the blister radius increases, which can lead to uncontrolled catastrophic debonding (Lai and Dillard, 1994). Furthermore, the pressurized test, which requires a sophisticated experimental setup to monitor the simultaneous change in pressure and blister dimension, suffers from the soft compliance of the gaseous medium and possible dissolved gases (Wan, 1999). To circumvent the problem of uncontrolled failure, many researchers have proposed some modified blister geometries, including the "constrained blister" (Chang et al., 1989), "island blister" (Allen and Senturia, 1989), "peninsula blister" (Dillard and Bao, 1991), and "stable pressurized blister test" (Wan and Mai, 1995a). It is also worthwhile to mention that the "shaft-loaded blister test", which utilizes the controlled displacement of a spherically capped shaft, driven, for example, by a universal testing machine, is an alternative to pressurized tests because better compliance measurements can be obtained (Jennings et al., 1995; Wan, 1999). However, one drawback of this technique is the large membrane stress in the vicinity of the blister center where the shaft is applied, which leads to plastic yielding or even film rupture (Wan and Mai, 1995b; Wan and Mai, 1996).

Another common test that has also been used in a variety of configurations is the peel test, in which a thin, flexible strip is pulled away at some angle from the underlying substrate. Peel tests are widely used for measuring the adhesion of flexible thin films and coatings, and extensive work has already been documented (Gent and Hamed, 1977; Kendall, 1971; Thouless and Jensen, 1992; Williams, 1993, 1997). Although the peel test offers a simple test geometry for measuring bond fracture strength, it still suffers from several problems. The most severe one is that if the coating is thin and the adhesion is strong, the coating may tear due to the high membrane/bending stresses at the debond tip or contact with the mechanical grips (Lai and Dillard, 1996, 1997; Wan et al., 2003).

One possible remedy to reduce the local stress concentration is to use low angle peel tests, as they increase the likelihood of debonding without film rupture or yielding (Gent and Kaang, 1986; Wan, 1999). One example of a low angle peel test is the pulloff test introduced by Gent and Kaang (1986). In this test, two opposite ends of the film are adhered to the sides of an opening in the substrate, while the other two edges remain free. An external line force is then applied via a horizontal bail underneath the film, so that the load is evenly distributed along the film width and the film deforms into inverted "V" shape. Gent and Kaang only considered the pull-off test for a thin flexible coating under pure stretching. Referring to this geometry as the V-peel test, Wan (1999) developed a closed form analytical solution of load vs. deflection by generating a parametric plot using the concomitant membrane stress as the independent variable. This model can account for the entire deformation range of the thin film, from bending plate to stretching membrane, in the absence of residual stress. Furthermore, the mechanics of thin film delamination from the rigid substrate and the corresponding strain energy release rate was derived without residual stress.

In this paper, we first discuss the load–deflection constitutive relation for the pull-off test considering tensile residual stress in the film, because many polymer coatings are pre-stressed in tension due to thermal misfit strains when cool down from the cure temperature (Yu and Hutchinson, 2003). Residual stresses also

constitute a driving force for interfacial delamination and assist in the delamination process. An accurate closed-form analytical solution for calculating the strain energy release rate at various residual stresses is also developed from the constitutive relation using a fracture mechanics approach. In order to verify our analytical model, a two-dimensional geometrically nonlinear FEA is also carried out to simulate the pull-off test, and the energy release rate is obtained numerically by using the modified crack-closure method (MCCM) (Rybicki and Kanninen, 1977; Raju et al., 1988; Sun and Qian, 1997). Finally, the contributions of two fracture modes, the opening mode and sliding mode, with the deflection and residual stress of the thin film, is investigated based upon FEA results.

2. Theory

In this section, we will present the analytical solution of both the constitutive relation (load vs. deflection) and delamination (strain energy release rate) considering the residual stress within the film.

2.1. Constitutive relation

As schematically shown in Fig. 1, a thin film of length, 2ℓ, thickness, h, Young's modulus, E, and Poisson's ratio, v, is pre-stressed by a uniform tensile residual stress of σ_r and adhered to a rigid substrate. Since film thickness and film length are considered much smaller than the width of the strip, a plane strain state is considered. An external load, F, is applied to the centerline of the strip via a horizontal bail of small cross-sectional radius, deflecting the film into an inverted "V" shape under a mixed bending/stretching mode. The film profile is denoted by $w(x)$ with a central deflection of w_0. When the slope of the film is small, the corresponding governing equation is given by Wan et al. (in press)

$$\frac{d^2w}{dx^2} - \frac{N}{D}w = -\frac{F}{2D}x - \frac{M_0}{D} \tag{1}$$

where x is the distance from one clamped end, $D = Eh^3/12(1-v^2)$ is the flexural rigidity, $M_0 = M|_{x=0}$ is the bending moment per unit width at one clamped end, and N is the resultant membrane force per unit width in the film, which is given by

$$N = \sigma h = (\sigma_m + \sigma_r)h \tag{2}$$

where σ is the resultant membrane stress and σ_m is the concomitant stress caused by the film deformation. The boundary conditions for this pull-off test are: (i) $w = dw/dx = 0$ at $x = 0$ and (ii) $dw/dx = 0$ at $x = \ell$. For the sake of convenience, a set of useful dimensionless variables are defined as follows: $\xi = x/\ell$,

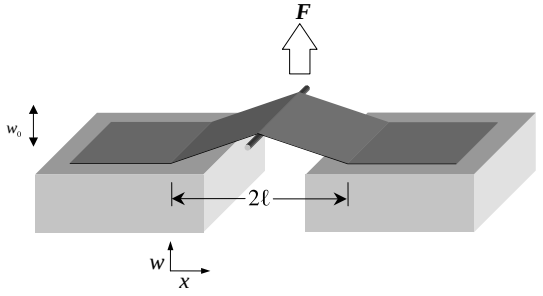

Fig. 1. Schematic of the pull-off test (w_0 is the central deflection. The film width is assumed to be much larger than 2ℓ.).

$\omega = w/h$, $\phi = F\ell^3/2Dh$, $\beta_m = (\sigma_m h\ell^2/D)^{1/2}\beta_r = (\sigma_r h\ell^2/D)^{1/2}$, and $\beta = (\sigma h\ell^2/D)^{1/2}$ where β is the dimensionless resultant membrane stress and $\beta^2 = \beta_r^2 + \beta_m^2$ from Eq. (2). Here β gauges the ratio of the resultant membrane stress to bending moment. After introducing the boundary conditions mentioned earlier, the deformed normalized film profile is

$$\omega = \frac{\phi}{\beta^3}\left\{ -\sinh(\beta\xi) + \frac{\cosh\beta - 1}{\sinh\beta}[\cosh(\beta\xi) - 1] + \beta\xi \right\} \tag{3}$$

with a normalized central deflection given by ($\xi = 1$)

$$\omega_0 = \frac{\phi}{\beta^3}\left\{ \beta - 2\tanh\frac{\beta}{2} \right\} \tag{4}$$

Wan et al. (in press) showed that an easy way to find the constitutive relation is to generate a parametric plot of $\phi(\beta_m, \beta_r)$ vs. $\omega_0(\beta_m, \beta_r)$ by varying the parameter β_m. Fig. 2 shows $\phi(\omega_0)$ as solid lines for fixed values of $\beta_r = 0$, 5, 10, and 20.

Wan (1999) also showed that when $\beta_m \to 0 (\beta \approx \beta_r)$, ω_0 is small and bending predominates. At this stage, ϕ increases linearly with ω_0. Thus, Eq. (4) is simplified to

$$\phi = k(\beta_r)\omega_0 \tag{5}$$

where

$$k(\beta_r) = \frac{\beta_r^3}{\beta_r - 2\tanh\frac{\beta_r}{2}} \tag{6}$$

Eq. (5) will reduce to $\phi = 12\omega_0$ in the absence of residual stress ($\beta_r = 0$). The film becomes stiffer with an increase of residual stress, and corresponds to a larger stiffness, k, and an upward shift of the ϕ-intercept in Fig. 2 (in log–log scale, all the curves at this stage are parallel to each other). It should be kept in mind that at large β_r the film deformation is dominated by the stretching residual stress instead of the bending moment, leading to a profile similar to that of pure stretching even at small deflection. We will discuss the effect of residual stress on the film profile in detail later in Section 4. On the other hand, if β_m is very large and ω_0 is also large, the residual stress becomes negligible compared to the overwhelming concomitant stress, $\beta_m \gg \beta_r$, and $\beta \approx \beta_m$. In this case, the constitutive relation approaches the stretching "cubic limit"

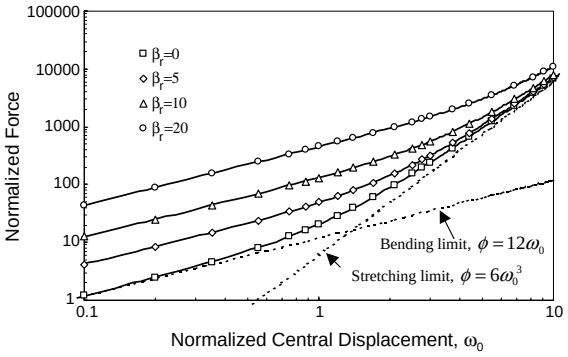

Fig. 2. Constitutive relation of normalized load ϕ as a function of normalized central deflection ω_0 at various β_r as indicated. The analytical solutions are shown as solid lines and FEA results are shown as data points. The linear ($\phi = 12\omega_0$) and cubic ($\phi = 6\omega_0^3$) asymptotes are shown as dotted lines.

$\phi = 6\omega_0^3$, which is independent of β_r. In other words, all $\phi(\omega_0)$ with any β_r converge to the same asymptote cubic line as shown in Fig. 2.

For an intermediate β_m, the deformed film is in the linear–cubic (bending–stretching) transition range. The linear to cubic transition location is estimated to occur at the intersection of the large $\omega_0(\phi = 6\omega_0^3)$ and small ω_0 (Eq. (5)) given by

$$\omega_0^* = \left[\frac{\beta_r^3}{6(\beta_r - 2\tanh(\beta_r/2))}\right]^{1/2} \tag{7}$$

Fig. 3 shows the increase of ω_0^* with β_r and the value of ω_0^* serves as a rough guide to determine whether the linear or cubic $\phi(\omega_0)$ is a better approximation. For $\beta_r = 0$, this transition occurs at $\omega_0^* = \sqrt{2} \approx 1.414$ and $\phi = 12\sqrt{2} \approx 16.97$.

2.2. Fracture mechanics of delamination

2.2.1. No residual stress case

When the central deflection or the applied force reaches a threshold, delamination occurs. The elastic strain energy, U_e, for a pull-off test is given by

$$U_e = \int_0^{w_0} F\,\mathrm{d}w_0 \tag{8}$$

Since $F = 2Dh\phi/\ell^3$ and $w_0 = \omega_0 h$, Eq. (8) can be rewritten as

$$U_e = \frac{2Dh^2}{\ell^3}\int_0^{\omega_0} \phi\,\mathrm{d}\omega_0 \tag{9}$$

Since $\beta_r = 0$, $\beta = \beta_m$, $\phi = \phi(\beta_m)$, and $\omega_0 = \omega_0(\beta_m)$. We have

$$U_e = \frac{2Dh^2}{\ell^3}\int_0^{\beta_m} \phi(\beta'_m)\frac{\mathrm{d}\omega_0}{\mathrm{d}\beta'_m}\mathrm{d}\beta'_m = \frac{2Dh^2}{\ell^3}\Phi(\beta_m) \tag{10}$$

where

$$\Phi(\beta_m) = \int_0^{\beta_m} \phi(\beta'_m)\frac{\mathrm{d}\omega_0}{\mathrm{d}\beta'_m}\mathrm{d}\beta'_m \tag{11}$$

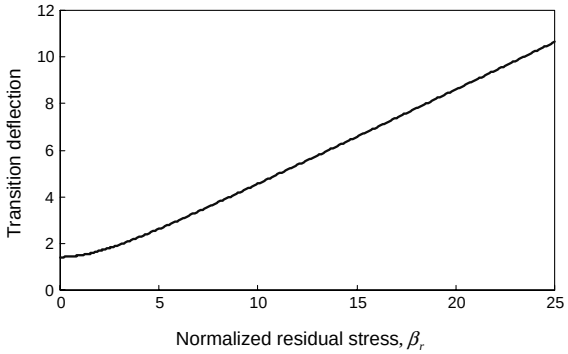

Fig. 3. Linear to cubic transition nondimensional deflection at various β_r.

The energy release rate, G, under a fixed displacement (central deflection, $dw_0 = 0$) is defined as

$$G = -\left.\frac{dU_e}{dA}\right|_{W_0} = -\left.\frac{dU_e}{2d\ell}\right|_{W_0} \tag{12}$$

where $A = 2\ell$ for the thin film strip per unit width.

Substituting Eq. (10) into (12), one obtains

$$G = \frac{3Dh^2}{\ell^4}\Phi(\beta_m) - \frac{Dh^2}{\ell^3}\frac{d\Phi(\beta_m)}{d\beta_m}\frac{d\beta_m}{d\ell} \tag{13}$$

Since $d\omega_0 = 0$ and $\omega_0 = \omega_0(\beta_m)$, $d\beta_m = 0$. It follows that the second term of Eq. (13) vanishes. Thus, the strain energy release rate in the absence of residual stress is

$$G = \frac{3Dh^2}{\ell^4}\Phi(\beta_m) \tag{14}$$

For the sake of convenience, a normalized energy release rate, χ, can be defined such that

$$\chi = G/(FW/2\ell) = \frac{3\Phi(\beta_m)}{\phi\omega_0} \tag{15}$$

From Eq. (15), the normalized energy release rate, χ, is only a function of β_m. Therefore, $\chi(\omega_0)$ and $\chi(\phi)$ can also be generated by parametric plots with respect to β_m, as shown in Figs. 4 and 5, respectively.

When the central deflection is small compared to the film thickness, as mentioned before, the constitutive relation is linear and $\phi = 12\omega_0$. It can easily be shown from Eqs. (11), (14) and (15) that $\chi = 1.5$. On the other hand, if the central deflection is very large compared to the film thickness, the cubic membrane behavior will be dominant, and the corresponding constitutive relation turns out to be $\phi = 6\omega_0^3$. In this case, it can also be shown that $\chi = 0.75$, which coincides with the solution given by Gent and Kaang (1986).

2.2.2. Tensile residual stress case

Since many polymer thin films are subjected to tensile residual stresses, effects of residual stress need to be considered for thin film delamination. The elastic strain energy, U_e, for a pull-off test with fixed tensile residual stress, σ_r, is given by

$$U_e = \frac{2Dh^2}{\ell^3}\int_0^{\omega_0}\phi\, d\omega_0 = \frac{2Dh^2}{\ell^3}\int_0^{\beta_m}\phi(\beta'_m,\beta_r)\frac{\partial\omega_0(\beta'_m,\beta_r)}{\partial\beta'_m}d\beta'_m = \frac{2Dh^2}{\ell^3}\Gamma(\beta_m,\beta_r) \tag{16}$$

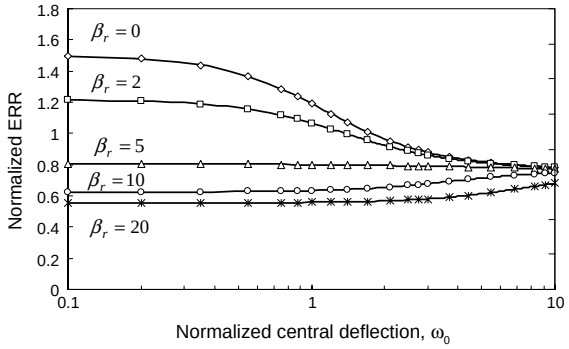

Fig. 4. Normalized strain energy release rate χ vs. normalized central deflection ω_0 at various β_r as indicated. The analytical solutions are shown as solid lines and FEA results are shown as data points. (ERR represents energy release rate.)

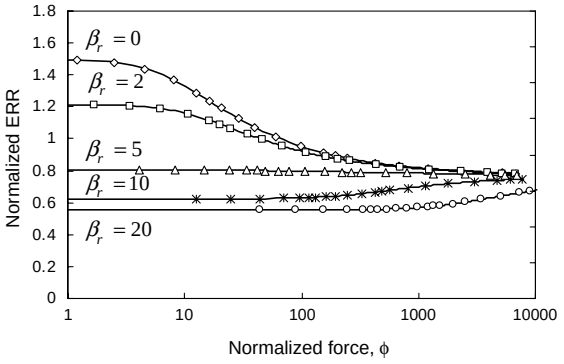

Fig. 5. Normalized strain energy release rate χ vs. normalized force ϕ at various β_r as indicated. The analytical solutions are shown as solid lines and FEA results are shown as data points. (ERR represents energy release rate.)

where

$$\Gamma(\beta_m, \beta_r) = \int_0^{\beta_m} \phi(\beta'_m, \beta_r) \frac{\partial \omega_0(\beta'_m, \beta_r)}{\partial \beta'_m} d\beta'_m \tag{17}$$

Since $\beta_r = (\sigma_r h l^2/D)^{1/2}$, at fixed σ_r, it can be shown that

$$\frac{d\beta_r}{d\ell} = \frac{\beta_r}{\ell} \tag{18}$$

The corresponding strain energy release rate is

$$\begin{aligned} G &= -\frac{dU_e}{dA}\bigg|_{\omega_0} = \frac{3Dh^2}{\ell^4}\Gamma(\beta_m, \beta_r) - \frac{Dh^2}{\ell^3}\frac{d\Gamma(\beta_m, \beta_r)}{d\ell} \\ &= \frac{3Dh^2}{\ell^4}\Gamma(\beta_m, \beta_r) - \frac{Dh^2}{\ell^3}\left(\frac{\partial \Gamma}{\partial \beta_r}\frac{d\beta_r}{d\ell} + \frac{\partial \Gamma}{\partial \beta_m}\frac{d\beta_m}{d\ell}\right) \end{aligned} \tag{19}$$

where

$$\frac{\partial \Gamma}{\partial \beta_r} = \int_0^{\beta_m} \frac{\partial\left[\phi(\beta'_m, \beta_r)\frac{\partial \omega_0(\beta'_m, \beta_r)}{\partial \beta'_m}\right]}{\partial \beta_r} d\beta'_m \tag{20}$$

and

$$\frac{\partial \Gamma}{\partial \beta_m} = \phi \partial \omega_0(\beta_m, \beta_r)/\partial \beta_m \tag{21}$$

Since $\omega_0 = \omega_0(\beta_m, \beta_r)$, at fixed ω_0,

$$d\beta_m = -\frac{\partial \omega_0/\partial \beta_r}{\partial \omega_0/\partial \beta_m} d\beta_r \tag{22}$$

Substituting Eq. (22) into Eq. (19), we have

$$G = \frac{3Dh^2}{\ell^4}\Gamma(\beta_m, \beta_r) - \frac{Dh^2}{\ell^3}\left(\frac{\partial \Gamma}{\partial \beta_r}\frac{d\beta_r}{d\ell} - \frac{\partial \Gamma}{\partial \beta_m}\frac{\partial \omega_0/\partial \beta_r}{\partial \omega_0/\partial \beta_m}\frac{d\beta_r}{d\ell}\right) \tag{23}$$

Substituting Eqs. (18) and (21) into Eq. (23),

$$G = \frac{3Dh^2}{\ell^4}\Gamma(\beta_m, \beta_r) - \frac{Dh^2}{\ell^4}\beta_r\left(\frac{\partial\Gamma}{\partial\beta_r} - \phi\frac{\partial\omega_0}{\partial\beta_r}\right) \tag{24}$$

Eq. (24) indicates that the energy release rate is a function of thin film deformation, β_m, residual stress, β_r, half of debond length, ℓ, material properties, such as E and v, and film thickness, h. Therefore, the normalized energy release rate, χ, is given by

$$\chi = G/(FW_0/2\ell) = \frac{3\Gamma}{\phi\omega_0} - \beta_r\frac{\partial\Gamma/\partial\beta_r}{\phi\omega_0} + \beta_r\frac{\partial\omega_0/\partial\beta_r}{\omega_0} \tag{25}$$

When the residual stress is equal to zero, Eq. (25) simplifies to Eq. (15) for the case with no residual stress.

Since Γ, ϕ, ω_0 are all functions of β_m and β_r, χ is also a function of β_m and β_r. Therefore, $\chi(\omega_0)$ and $\chi(\phi)$ can be generated by parametric plots with respect to β_m at various β_r as shown in Figs. 4 and 5, respectively.

For $\beta_m \to 0$, $\beta \approx \beta_r$, both ϕ and ω_0 are small, and $\phi(\omega_0)$ is linear. Substituting Eq. (5) into Eq. (25),

$$\chi_0 = \frac{\beta_r\tanh^2(\beta_r/2)}{2\beta_r - 4\tanh(\beta_r/2)} \tag{26}$$

which determines the downward shift of χ_0 in Figs. 4 and 5 with the increase of β_r. Note that $1/2 \leqslant \chi_0 \leqslant 3/2$ with the lower and upper limits corresponding to $\beta_r \to \infty$ and $\beta_r = 0$, respectively. In the limit of $\beta_m \to \infty$, $\beta_m \gg \beta_r$, and $\hat{\beta} \approx \beta_m$, both ω_0 and ϕ are large. Therefore, $\phi(\omega_0)$ is essentially cubic and χ approaches $\chi_\infty = 3/4$, regardless of β_r. An intermediate $\beta_m \approx \beta_r$ requires χ to fall between χ_0 to χ_∞ and the linear–cubic transition shifts to a higher ω_0 and ϕ as β_r increases.

3. Finite element analysis

In order to verify the preceding analytical models of the constitutive relation and the energy release rate, a geometrically nonlinear FEA was conducted using the commercial general FEA package ANSYS®. In the FEA model, the substrate was modeled as a rigid body and was not subject to any deformation because the thickness and stiffness of the substrate are generally much greater than those of the film. A linear elastic model of a generic polymer with $E = 3.4$ GPa and $v = 0.32$ was used for the thin film. The ratio between the debond length, 2ℓ, and the film thickness, h, is equal to 100 (4000 μm/40 μm) to simulate the actual geometry of thin films being studied in our laboratory. Taking advantage of the symmetry of geometry and assuming the width of the film to be much larger than the film thickness, a geometrically nonlinear, two-dimensional plane strain FEA model was generated for half of the test geometry to characterize the full deformation range of the thin film behavior from pure bending to pure stretching at various residual stress levels. A total of 6300 four-node isoparametric elements were used in this analysis and the mesh near the delamination front is shown in Fig. 6. Biased meshes were constructed except for the regions near the delamination front and the applied load to save memory space and computing time without losing accuracy. Different tensile residual stresses were introduced by first subjecting the thin film to uniform temperature changes. Basically, the FEA simulated fixed displacement condition and the central displacement, w_0, was varied from 0.1 to 10 h to cover the full deformation range. For each specific central deflection, w_0, the corresponding force was obtained by the reaction force at the same node.

In order to extract the energy release rate, the MCCM (Rybicki and Kanninen, 1977; Raju et al., 1988; Sun and Qian, 1997) was employed based on Irwin's theory (1958) that if a crack extends by a small amount, $\Delta\ell$, compared to the original crack length, ℓ, the strain energy released in this process is equal to the work needed to close the crack to its original length. In terms of the finite element representation, we have

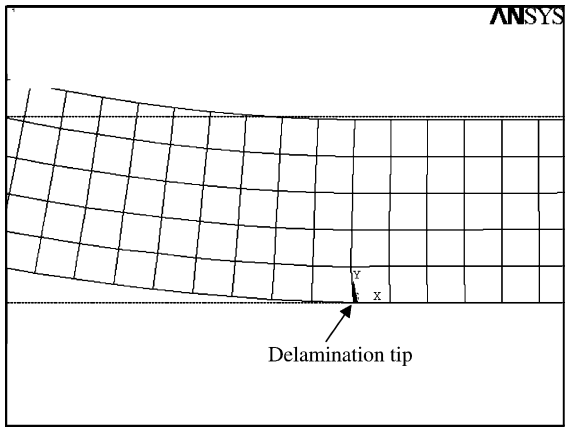

Fig. 6. Close-up views of FEA mesh near the delamination tip.

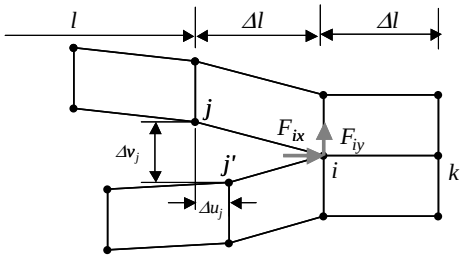

Fig. 7. Schematic of MCCM (i is the crack tip).

$$G = G_{\mathrm{I}} + G_{\mathrm{II}} \tag{27}$$

$$G_{\mathrm{I}} = -\frac{1}{2\Delta\ell} F_{iy} \cdot \Delta v_j \tag{28}$$

$$G_{\mathrm{II}} = -\frac{1}{2\Delta\ell} F_{ix} \cdot \Delta u_j \tag{29}$$

where F_{ix} and F_{iy} are the shear and opening forces at node i, and Δu_j and Δv_j are the shear and opening displacements at node j as shown in Fig. 7. Results of the constitutive relation and the energy release rate from the FEA have been shown in the corresponding graphs presented above, such as Figs. 2, 4 and 5, to allow comparisons with the analytical solutions. Obviously, the analytical results for both the constitutive relation and the energy release rate are in excellent agreement with the FEA data.

4. Discussion

4.1. Insights of thin film deformation from pull-off test

The analytical solutions proposed herein for the pull-off test geometry are useful for characterizing the constitutive behavior and interfacial delamination of thin films. This model captures the full deformation

range of thin films spanning from linear plate bending to cubic membrane behavior, including a smooth transition between these two limiting regimes. The plane strain solutions are presented here assuming that the width of the strip is large compared to the thickness of the film, and the plane stress solutions can be easily obtained as well by replacing E' (i.e. $E/1-v^2$) by E (i.e. D by $D(1-v^2)$).

In order to derive the constitutive relation and the energy release rate, parametric plots are used to circumvent the involved mathematics for solving the transcendental equations. The normalized applied load, ϕ, the normalized central displacement, ω_0, and the normalized energy release rate, χ, are all functions of the normalized membrane stress, β_m and the normalized residual stress, β_r.

Residual stresses play an important role in both the constitutive relation and the energy release rate. At small deflections, increasingly tensile residual stresses serve to make films stiffer due to the additional restoring force resulting from the residual stress. Fig. 2 also shows that at large residual stress the transition to cubic stretching-dominated regime is delayed since the deformation related stress, β_m, must be large enough to dominate the residual stress β_r. With the increase of deflections, residual stress effects become less pronounced and finally all the constitutive curves approach the same asymptote, which is the cubic stretching limit given earlier.

The normalized energy release rate, χ, is defined as the ratio of the applied energy release rate, G, to a work-like term, Fw_0, divided by a characteristic length dimension. For the pull-off test geometry without residual stress, χ ranges from 3/2 in the linear region to 3/4 in the cubic stretching region, which is consistent with Gent's solution (1986). As shown earlier, when the deflection is very small, χ varies from 1/2 to 3/2 depending on the residual stress within the film. On the other hand, the residual stress does not significantly affect χ at large displacements and χ approaches 3/4 eventually, regardless of the value of the residual stress because the membrane stress prevails at large deflections.

4.2. Comparison between analytical solutions and FEA

Fig. 2 shows that the constitutive relations obtained by the analytical solutions agree very well with the FEA results for the whole deformation region at various residual stresses. Since a small angle assumption is included in the analytical solutions, we expect that larger deviation of analytical solutions from FEA results could occur at larger deflections. For example, when the normalized central deflection, ω_0, is equal to 10, the relative deviations of the normalized load, ϕ, from FEA results are only 0.4% without residual stress and 0.6% for β_r equal to 20.

In order to distinguish the bending and stretching state of thin films directly, and check the accuracy of the analytical model for the pull-off test geometry at different central deflections and residual stresses, the deflection profiles are obtained from both analytical solutions and FEA. Fig. 8 shows a comparison of the normalized thin film deflection profiles for the analytical solutions and FEA results at three normalized central deflection values without residual stress. Fig. 9 shows the comparison for $\beta_r = 20$. Fig. 8 indicates that when there is no residual stress within the film and the central deflection is small compared to the thickness of the film (i.e. $\omega_0 = 0.1$), the deflection profile is sigmoidal in shape implying that the bending effects are quite significant. With an increase of the central deflection, the shapes of profiles change from sigmoidal to a straight line, showing increasing cubic stretching effects and decreasing bending effects, which agrees with our analytical solutions given earlier. Interestingly, Fig. 9 shows that if the thin film is pre-stressed by the tensile residual stress, even when the central deflection is very small compared to the film thickness, the shape of the profile already approximates a straight line because of the stretching residual stress effect. We should keep in mind that this stretching effect due to the tensile residual stress is different from the cubic stretching effect mentioned earlier, because the former is linear in terms of load vs. deflection and the later is cubic caused by the large film deflection.

Figs. 4 and 5 show the normalized energy release rate, χ, from both analytical solutions and FEA. Obviously, excellent agreement is achieved at various residual stress values, and residual stress effects are

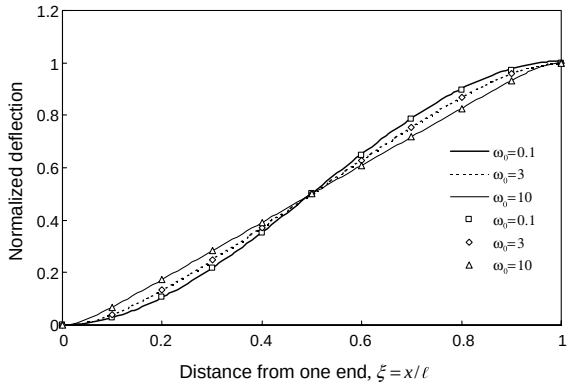

Fig. 8. Normalized deflection profiles of pull-off test for $\beta_r = 0$. Analytical solutions are shown as lines, and FEA as data points.

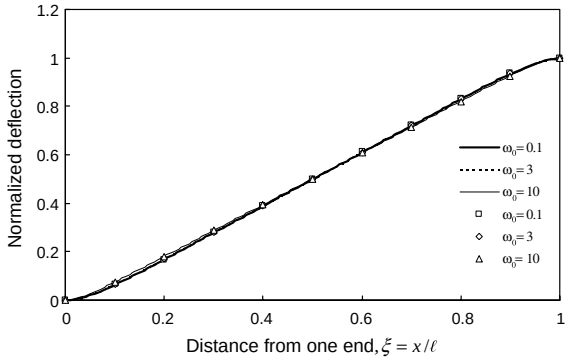

Fig. 9. Normalized deflection profiles of pull-off test for $\beta_r = 20$. Analytical solutions are shown as lines, and FEA as data points.

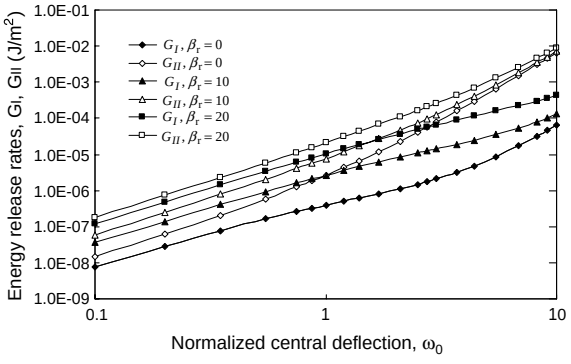

Fig. 10. Fracture energy release rates of pull-off test at various residual stresses.

significant at small deflection range and control the shift of the curves. On the other hand, residual stress effects diminish with the increase of the load or deflection and eventually the values of χ at all different

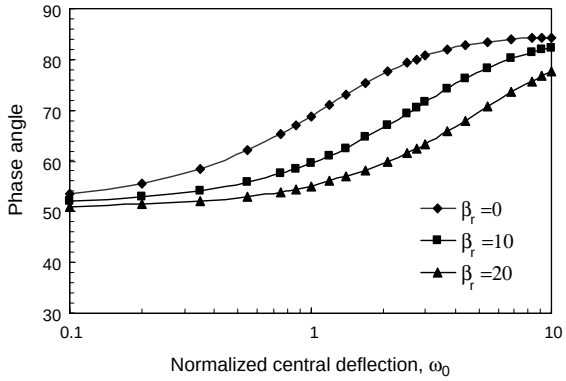

Fig. 11. Phase angle as a function of normalized central deflection for various residual stresses.

residual stresses approach the membrane solution given by Gent and Kaang (1986) and Williams (1997). Again at a normalized central deflection, ω_0, equal to 10, the relative deviations of χ from FEA results are only 0.1% without residual stress and only 0.05% for β_r equal to 20.

4.3. Fracture mode analysis of pull-off test

In our FEA model using the MCCM, we can also extract the individual strain energy release rates, G_I and G_{II} from Eqs. (28) and (29) under a finite crack extension (Sun and Qian, 1997). Fig. 10 shows G_I and G_{II} vs. central deflections at various β_r. Obviously, both mode I and mode II energy release rates increase monotonously with the central deflection, and at the same deflection, higher residual stress accounts for higher energy release rate. At one specific β_r, mode II always dominates mode I and this scenario becomes more and more significant with the transition of film deformation from linear regime to cubic stretching regime. If there is no elastic mismatch between the film and substrate, i.e., the Dundurs' parameters, $\hat{\alpha}$ and $\hat{\beta}$, are both equal to zero, the phase angle Ψ is given by $\Psi = \tan^{-1}(K_{II}/K_I) = \tan^{-1}\sqrt{G_{II}/G_I}$. Fig. 11 shows the phase angle change at various residual stresses. The phase angle also increases monotonically with the central deflection, which confirms the increasing dominance of mode II when the film approaches the cubic stretching regime. With an increase of residual stress, the mode ratio increase is delayed due to residual stress effects. Generally speaking, for the peel test, both the local moment and membrane force near the crack tip contribute to the energy release rate given by Hutchingson and Suo (1992). Since the pull-off test is a low angle peel test, the continuously increasing membrane force caused by the pull-off test will contribute primarily to mode II fracture and this effect will become dominant once the film enters the cubic stretching regime. It is also worthwhile to mention that the effect of residual stress on fracture modes diminishes when the deflection is large, because in the cubic stretching region, β_m dominates β_r and the residual stress is overshadowed by the membrane stress.

5. Conclusions

A closed-form analytical solution for the interfacial delamination is developed for the pull-off test. The solutions accurately predict the full deformation of thin films ranging from linear bending to cubic stretching and coincide with the two limiting cases: linear load–deflection behavior when bending or large residual stresses dominate, and cubic behavior where stretching is dominant. Since this model can also

capture the transition region, the constitutive solution and the derived deflection profile are not only useful in modeling the behavior of films, coatings, or tapes subjected to this test geometry, but also may be employed to determine residual stresses and material properties.

An accurate closed-form solution for the strain energy release rate is derived based upon the constitutive solution using a fracture mechanics approach. Both the constitutive solution and the energy release rate solution are shown to agree very well with the FEA results at various residual stress values. The analytical model and FEA show that residual stresses play an important role in both the constitutive relation and the energy release rate, and the effects become less pronounced when the deformation of the film approaches the cubic stretching region, where the membrane stress dominates the residual stress. Finite element analysis results suggest that the mode II energy release rate is dominant as far as the test geometry and the deformation region are considered, and this fracture mode analysis could be useful for studying mixed-mode thin film delamination problem.

Acknowledgements

The authors would like to acknowledge the support of the Hewlett-Packard Corporation and the Engineering Science and Mechanics Department at Virginia Tech. We are also grateful to the Center for Adhesive and Sealant Science at Virginia Tech for fostering interdisciplinary research in adhesion science.

References

Allen, M.G., Senturia, S.D., 1989. Application of the island blister test for thin film adhesion measurement. Journal of Adhesion 29, 219–231.

Bennett, S.J., Devries, K.L., Williams, L.M., 1974. Adhesive fracture mechanics. International Journal of Fracture 10 (1), 33–43.

Chang, Y.S., Lai, Y.H., Dillard, D.A., 1989. The constrained blister—a nearly constant strain-energy release rate test for adhesives. Journal of Adhesion 27, 197–211.

Cotterell, B., Chen, Z., 1997. The blister test-transition from plate to membrane behavior for an elastic material. International Journal of Fracture 86, 191–198.

Dannenberg, H., 1961. Measurement of adhesion by a blister method. Journal of Applied Polymer Science 5, 125–134.

Dauskardt, R.H., Lane, M., Ma, Q., Krishna, N., 1998. Adhesion and debonding of multi-layer thin film structures. Engineering Fracture Mechanics 61, 141–162.

Dillard, D.A., Bao, Y., 1991. The peninsula blister test: a high and constant strain energy release rate fracture specimen for adhesives. Journal of Adhesion 33, 253–271.

Gent, A.N., Hamed, G.R., 1977. Peel mechanics for an elastic–plastic adherend. Journal of Applied Polymer Science 21, 2817–2831.

Gent, A.N., Kaang, S., 1986. Pull-off forces for adhesive tapes. Journal of Applied Polymer Science 32, 4689–4700.

Gent, A.N., Lewandowski, L.H., 1987. Blowing-off pressures for adhering layers. Journal of Applied Polymer Science 33, 1567–1577.

Hutchingson, J.W., Suo, Z., 1992. Mixed mode cracking in layered materials. Advances in Applied Mechanics 29, 63–191.

Irwin, G.R., 1958. Fracture mechanics. In: Structure Mechanics: Proceedings of the 1st Symposium on Naval Structural Mechanics. Pergamon Press, New York, pp. 557–591.

Jennings, R.M., Taylor, J.F., Farris, R.J., 1995. Determination of residual stress in coatings by a membrane deflection technique. Journal of Adhesion 49, 57–74.

Jensen, H.M., Thouless, M.D., 1993. Effects of residual stresses in the blister test. International Journal of Solids and Structures 30 (6), 779–795.

Kendall, K., 1971. The adhesion and surface energy of elastic solids. Journal of Physics D: Applied Physics 4, 1186–1195.

Lai, Y.H., Dillard, D.A., 1994. A study of the fracture efficiency parameter of blister tests for films and coatings. Journal of Adhesion Science and Technology 8 (6), 663–678.

Lai, Y.H., Dillard, D.A., 1996. A comparison of energy release rates in different membrane blister and peel tests. Journal of Adhesion 56, 59–78.

Lai, Y.H., Dillard, D.A., 1997. Using the fracture efficiency to compare adhesion tests. International Journal of Solids and Structures 34 (4), 509–525.

Raju, I.S., Crews, I.H., Aminpour, M.A., 1988. Convergence of strain energy release rate components for edge-delaminated composite laminates. Engineering Fracture Mechanics 30, 383–396.

Rybicki, E.F., Kanninen, M.F., 1977. A finite element calculation of stress intensity factors by a modified crack closure integral. Engineering Fracture Mechanics 9, 931–938.

Sheplak, M., Dugundji, J., 1998. Large deflection of clamped circular plates under initial tension and transitions to membrane behavior. Journal of Applied Mechanics 65, 107–115.

Sun, C.T., Qian, W., 1997. The use of finite extension strain energy release rates in fracture of interfacial cracks. International Journal of Solids and Structures 34, 2595–2609.

Thouless, M.D., Jensen, H.M., 1992. Elastic fracture mechanics of the peel-test geometry. Journal of Adhesion 38, 185–197.

Wan, K.T., 1999. Fracture mechanics of a V-peel adhesion test—transition from a bending plate to a stretching membrane. Journal of Adhesion 70, 197–207.

Wan, K.T., Lim, S.C., 1998. The bending to stretching transition of a pressurized blister test. International Journal of Fracture 92, L43–47.

Wan, K.T., Mai, Y.W., 1995a. Fracture-mechanics of a new blister test with stable crack-growth. Acta Metallurgica et Materialia 43 (11), 4109–4115.

Wan, K.T., Mai, Y.W., 1995b. Fracture mechanics of a shaft-loaded blister of thin flexible membrane on rigid substrate. International Journal of Fracture 74, 181–197.

Wan, K.T., Mai, Y.W., 1996. Fracture mechanics of a shaft-loaded blister of thin flexible membrane on rigid substrate. International Journal of Fracture 74 (2), 181–197.

Wan, K.T., Guo, S., Dillard, D.A., 2003. A theoretical and numerical study of a thin clamped circular film under an external load in the presence of tensile residual stress. Thin Solid Films 425, 150–162.

Wan, K.T., Sun, Z., Dillard, D.A. 2003. Strain energy release rate of a thin pre-stressed film delaminating from a rigid substrate by a V-peel test. Thin Solid Films. in press.

Williams, J.G., 1993. Root rotation and plastic work effects in the peel test. Journal of Adhesion 41, 225–239.

Williams, J.G., 1997. Energy release rates for the peeling of flexible membrances and the analysis of blister tests. International Journal of Fracture 87, 265–288.

Williams, M.L., 1972. Relation of continuum mechanics to adhesive fracture. Journal of Adhesion 4, 307–332.

Yu, H., Hutchinson, J.W., 2003. Delamination of thin film strips. Thin Solid Films 423, 54–63.